Microporous and Mesoporous Materials 264 (2018) 176–180

Contents lists available at ScienceDirect

Microporous and Mesoporous Materials

journal homepage: www.elsevier.com/locate/micromeso

Evolution of porosity of activated carbon fibres prepared from pre-oxidized acrylic fibres

P.J.M. Carrott[a,*], M.M.L. Ribeiro Carrott[a], P.F.M.M. Correia[b]

[a] Centro de Química de Évora, Instituto de Investigação e Formação Avançada, Departamento de Química, Escola de Ciências e Tecnologia, Universidade de Évora, Colégio Luís António Verney, 7000-671 Évora, Portugal

[b] Fisipe SA, Member of SGL Group - The Carbon Company, Apartado 5, 2836-908 Lavradio, Portugal

ARTICLE INFO

Keywords:
Activated carbon fibre
Acrylic fibre
Microporosity
CO_2 capture
Micropore development

ABSTRACT

Industrially pre-oxidized acrylic fibres were used to prepare activated carbon fibres (ACF). The results obtained show that pre-oxidation was effective in increasing the carbon yield during carbonization and reducing the reactivity of the char with CO_2 during activation, making it possible to obtain ACF with high pore volumes, up to 1.15 $cm^3 g^{-1}$, with BET area of 2064 $m^2 g^{-1}$, even without a prior laboratory stabilization step. By controlling the activation temperature over the range 700–1000 °C and the activation time over the range 15–4320 min it was possible to obtain a range of materials varying from those which contained mainly ultramicropores, with a high capacity for the capture of CO_2, up to others with a broader distribution of pore sizes extending up to 4 nm. An interesting aspect of the results was the observation that the volume of ultramicropores was practically constant for different activation times and temperatures up to 900°C. The importance of different processes which may contribute towards the development of porosity during activation is considered in the light of the results obtained.

1. Introduction

In comparison with the traditional granular (GAC), powder (PAC) and extruded (EAC) grades of activated carbon, activated carbon fibres (ACF) combine a number of advantages, including high rates of adsorption, easy separation, uniform tailored porosity and purity. They are currently manufactured by a number of companies, principally from cellulosic, PAN (polyacrylonitrile), phenolic and pitch precursor fibres, and find application in various areas related to health, energy, and environmental control [1,2]. A major limitation to their more widespread use is their high cost compared to GAC/PAC/EAC. In this respect, PAN based ACF are one of the less expensive [3] which is at least partially due to the fact that PAN, or acrylic, is a major textile fibre and PAN is also the principal precursor for fabrication of high performance structural carbon fibres [4].

Polymer fibres may be produced by a fibre company and then converted to ACF by a carbon company. In the case of PAN or acrylic fibres, the first stage of ACF production involves stabilization of the fibres by heating under tension in an inert or oxidizing atmosphere [5]. Relatively recently, a range of acrylic fibre based “technical fibres” have been commercialized by Fisipe SA (Portugal, member of SGL Group - The Carbon Company). These include pre-oxidized acrylic fibres which in principle should not need to be stabilized by the ACF manufacturer prior to carbonization and activation, thereby reducing the manufacturing costs.

The production of ACF from this type of pre-oxidized fibre has not been reported before. Hence, the principal objectives of the work reported here were to assess the possibility of using them to prepare high surface area ACF with a view towards reducing the production costs of the ACF, and then to demonstrate the effect of systematically varying activation conditions on the pore structure of the materials obtained. In previous work [6] we prepared ACF from non-pre-oxidized acrylic textile fibres produced in the same factory but with stabilization under nitrogen in our laboratory prior to carbonization and activation in CO_2. Significant improvements were found in the present work. In addition, the importance of different processes which may contribute towards the development of porosity during activation is considered in the light of the results obtained.

Many works have been published on the development of porous materials for the capture of CO_2 [7–9] and in recent years good results have been obtained using activated carbons for the adsorption of CO_2 even at about 25°C and near atmospheric pressure [10–16]. Hence the materials obtained in this work were tested as adsorbents for the capture of CO_2.

* Corresponding author.
E-mail address: peter@uevora.pt (P.J.M. Carrott).

https://doi.org/10.1016/j.micromeso.2018.01.027
Received 26 October 2017; Received in revised form 12 December 2017; Accepted 18 January 2018

2. Materials and methods

The precursor used in this work was a pre-oxidized acrylic fibre specially prepared by Fisipe SA, member of SGL Group - The Carbon Company. For the preparation of the ACF, a vertical tube furnace and constant gas flow of 85 $cm^3 min^{-1}$ were used. Each sample was prepared from approximately 3 g of acrylic fibre carbonized by heating to 700, 800, 900 or 1000 °C at a rate of 10°C min^{-1} under N_2. Activation was carried out by switching to a CO_2 flow for between 15 and 4320 min, then switching back to the N_2 flow and allowing the sample to cool to below 50°C before removing from the furnace. The samples are designated FXtq, where t is the activation temperature in °C divided by 100°C and q is the burn-off. Each sample was subsequently characterized by adsorption of N_2 at 77 K using a Quantachrome Autosorb iQ after outgassing at 300°C for 5 h. The N_2 adsorption-desorption isotherms were analysed using the following: the Quenched Solid Density Functional Theory (QSDFT) model for the determination of pore size distribution [17]; the BET method for the determination of apparent specific surface area, A_{BET}, and C parameter, C, applied using the criteria recommended by Rouquerol et al. [18] and subsequently endorsed by IUPAC [19]; the α_s method for the determination of pore volume, v_s, and specific external surface area, A_s; the Dubinin-Astakhov (DA) equation for the determination of pore volume, v_o, and characteristic energy, E_o, which was subsequently converted to an estimate of mean pore size, L_o, from the relationship [20]:

$$L_o = 10.8/(E_o - 11.4)$$

The CO_2 adsorption and desorption performance of the samples was evaluated using a Perkin-Elmer STA6000 thermogravimetric analyzer. In this work, a CO_2/N_2 mixture was used for the measurements and its precise composition was determined using a Spectra Vacscan Plus quadrupole mass spectrometer with the tip of the capillary inlet placed as close as possible to the sample position. The CO_2 partial pressure was found to be 51 kPa. The sample, approximately 10 mg, was conditioned by heating at 300°C under a 100 $cm^3 min^{-1}$ flow of He. After cooling to 25°C the subsequent experimental program was: constant temperature for 5 min; switch from He to CO_2 and leave for 20 min; switch from CO_2 to He and leave for 60 min. Blank runs with no sample were carried out in order to correct for the change in buoyancy between He and the CO_2/N_2 mixture.

3. Results and discussion

3.1. Carbonization and activation

The carbonization yields decreased with increase in carbonization temperature, being 64, 60, 53 and 50% at 700, 800, 900 and 1000°C respectively. In previous work [6], where the acrylic fibres were stabilized in N_2 but not pre-oxidized, the carbonization yield at 800°C was found to be approximately 50%. The objective of stabilization is to promote the formation of cross-links and partial aromatization and to increase the average molar mass at relatively low temperatures. It follows that when the material is carbonized at higher temperatures the loss of volatile matter, due to chain scission, for example, will be lower. In addition, the cross-linked and aromatic structures formed will have a higher thermal stability than the C-C bonds of the linear polymer precursor. The significantly higher carbonization yield of 60% obtained in this work at 800°C indicates that the pre-oxidation was effective in stabilizing the fibres and hence in decreasing the loss of material during the carbonization.

The values of burn-off during subsequent activation are included in Table 1. At each activation temperature there was a linear increase in burn-off with increasing activation time. In the previous work, two distinct regimes of reactivity were observed, but this behaviour was not found here with the pre-oxidized fibres. A comparison of reactivity can be made by estimating the activation energies for activation from an Arrhenius plot. For this purpose, the slopes of the plots of burn-off as a function of activation time were used as a measure of rate of activation. It was found that the points at the three lowest temperatures gave a straight line and from the corresponding slope a value of 187 kJ mol^{-1} was obtained for the activation energy for activation of the carbonized fibres. The results previously obtained, only at the two temperatures 800 and 900°C, and for the first regime of (lower) reactivity, lead to a value of 163 kJ mol^{-1}. The higher value obtained in this work confirms that the pre-oxidation step resulted in the production of stabilized fibres with a reduced intrinsic reactivity.

Table 1
Sample preparation conditions, burn-offs, and pore volumes determined by the application of the QSDFT method to N_2 adsorption isotherms determined at 77 K.

Designation	Temperature/°C	Time/min	Burn-off/%	V_p (< 0.7 nm)/ $cm^3 g^{-1}$	V_p (0.7–4 nm)/ $cm^3 g^{-1}$
FX714	700	360	14	nd	nd
FX719	700	660	19	nd	nd
FX724	700	1002	24	nd	nd
FX735	700	1980	35	0.20	0.06
FX756	700	4320	56	0.24	0.16
FX817	800	60	17	0.11	0.04
FX829	800	150	29	0.18	0.07
FX843	800	300	43	0.22	0.12
FX862	800	480	62	0.22	0.27
FX871	800	660	71	0.20	0.42
FX911	900	20	11	nd	nd
FX934	900	60	34	0.20	0.12
FX944	900	80	44	0.20	0.24
FX960	900	120	60	0.19	0.46
FX983	900	150	83	0.21	0.64
FX1013	1000	15	13	0.07	0.06
FX1029	1000	30	29	0.13	0.14
FX1049	1000	45	49	0.15	0.29
FX1051	1000	60	51	0.17	0.41
FX1071	1000	72	71	0.13	0.59
FX1078	1000	90	78	0.14	0.99

V_p (< 0.7 nm), V_p (0.7–4 nm) – cumulative pore volumes corresponding to 0.7 nm and between 0.7 and 4 nm, obtained from the pore size distributions; nd – not determined.

3.2. Adsorption of N_2 at 77 K

Representative adsorption-desorption isotherms of N_2 at 77 K are shown in Fig. 1. Almost all of the isotherms determined on the different samples were found to be Type I of the IUPAC classification [19] with a

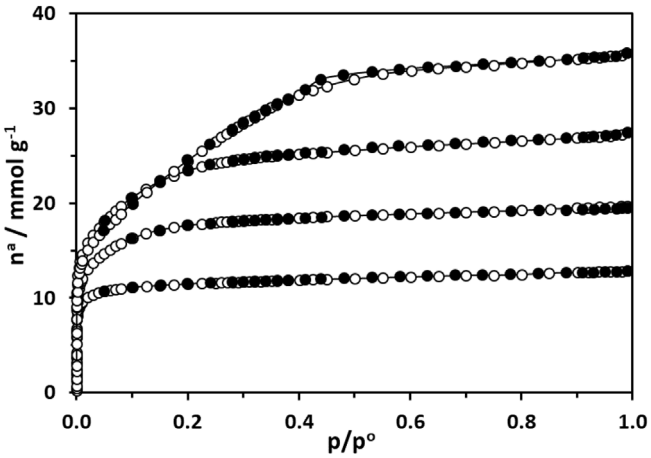

Fig. 1. Representative N_2 adsorption-desorption isotherms determined at 77 K. From top to bottom at 0.9 p^o – FX1078, FX983, FX871, FX756.

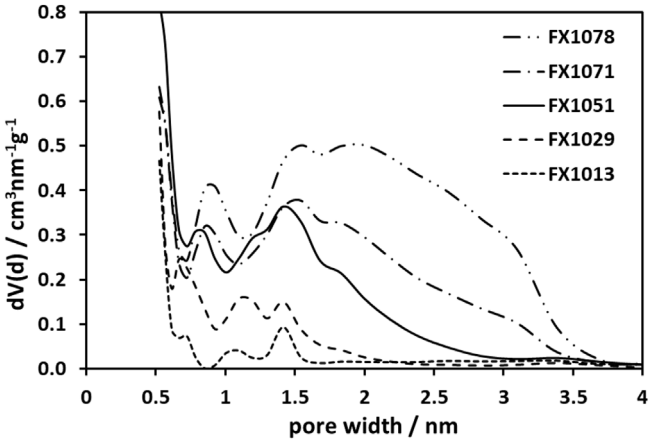

Fig. 2. QSDFT pore size distributions of samples prepared by activation at 1000°C.

progressive change from Type Ia to Type Ib as the burn-off increased. For two of the highest burn-off samples, FX1078 and FX1071, the isotherms had a very small hysteresis loop at approximately 0.4–0.6 p^o near the plateau of the isotherm. For four of the lowest burn-off samples, as well as the chars, the complete isotherms were not measured due to exceedingly long equilibrium times, indicating the presence of very narrow constrictions at the micropore entrances and slow diffusion of N_2 molecules at 77 K in very narrow ultramicropores.

Representative QSDFT [17] pore size distributions are shown in Fig. 2. In all cases the pore size distributions indicate a sharp peak below 0.7 nm corresponding to the presence of ultramicropores. For very low burn-off samples this was the predominant peak. However, as the burn-off increased, a second broader peak began to grow at wider pore widths, extending up to almost 4 nm for the highest burn-off sample at 1000°C, FX1078. For this sample the second peak accounted for 88% of the total pore volume. It is also instructive to compare the absolute values of pore volume given in Table 1. At each activation temperature the volume of pores between 0.7 nm and 4 nm in width increased significantly with increasing burn-off. In addition, considering similar burn-offs, the values increased with increasing activation temperature. In stark contrast to this behaviour, the volume of ultramicropores, with width < 0.7 nm, shows very little variation, neither with increasing burn-off nor at different activation temperatures (except at 1000°C, where the values are slightly lower). Similar behaviour has been found previously during physical activation of viscose rayon cloths [21] and the present results confirm the importance of taking into consideration the contribution of different processes towards the evolution of the pore structure during activation.

Table 2
Textural characteristics of samples obtained by analysis of N_2 adsorption isotherms determined at 77 K.

designation	$A_{BET}/m^2 g^{-1}$	C	$A_s/m^2 g^{-1}$	$v_s/cm^3 g^{-1}$	$v_o/cm^3 g^{-1}$	L_o/nm	n
FX735	651	2995	33	0.26	0.22	0.64	3.2
FX756	1009	1074	28	0.41	0.35	0.82	2.6
FX817	356	3015	24	0.17	0.14	0.62	3.9
FX829	618	2289	27	0.25	0.21	0.66	2.9
FX843	846	1334	23	0.35	0.29	0.76	2.6
FX862	1174	592	32	0.50	0.38	0.94	2.6
FX871	1495	205	33	0.64	0.51	1.24	2.1
FX934	790	1144	23	0.32	0.27	0.78	2.6
FX944	1038	598	31	0.44	0.35	0.97	2.4
FX960	1503	166	42	0.66	0.49	1.24	2.3
FX983	1942	118	48	0.87	0.61	1.35	2.2
FX1013	276	957	28	0.13	0.09	0.75	2.7
FX1029	645	537	16	0.28	0.22	0.93	2.3
FX1049	1014	212	28	0.45	0.33	1.07	2.2
FX1051	1271	184	36	0.59	0.40	1.18	2.4
FX1071	1424	81	44	0.73	0.46	1.56	2.1
FX1078	2064	49	61	1.15	0.63	1.78	2.1

A_{BET}, C – specific surface area and C parameter obtained by the BET method; A_s, v_s – specific external surface area and pore volume obtained by the α_s method; v_o, L_o, n – pore volume, mean pore width and n exponent determined by application of the DA Equation.

Fig. 3 is an extended version of the model originally presented in Ref. [21] which considers changes in the localised ordered regions of layer planes. At all stages of activation the more reactive carbon atoms are removed by "reaction" with the activating gas creating spaces which constitute the ultramicroporosity. Subsequently, "reorganization" of the localised ordered regions can occur and we propose that during physical activation of non-impregnated chars this will be the main process giving rise to the formation of supermicropores and small mesopores up to about 4 nm in size, that is, to the second peak in the pore size distribution. Alternatively, "collapse" of the structure may occur leading to some "pore widening" or contributing towards "shrinkage" of the structure. Continued shrinkage by this process will lead to "pore narrowing". In the case of ACF there appears to be a compensation between processes of micropore creation and pore narrowing which maintains the volume of ultramicropores fairly constant.

For purposes of comparison with other published work, where pore size distributions have often not been presented, parameters obtained by application of the BET, α_s and DA methods are given in Table 2.

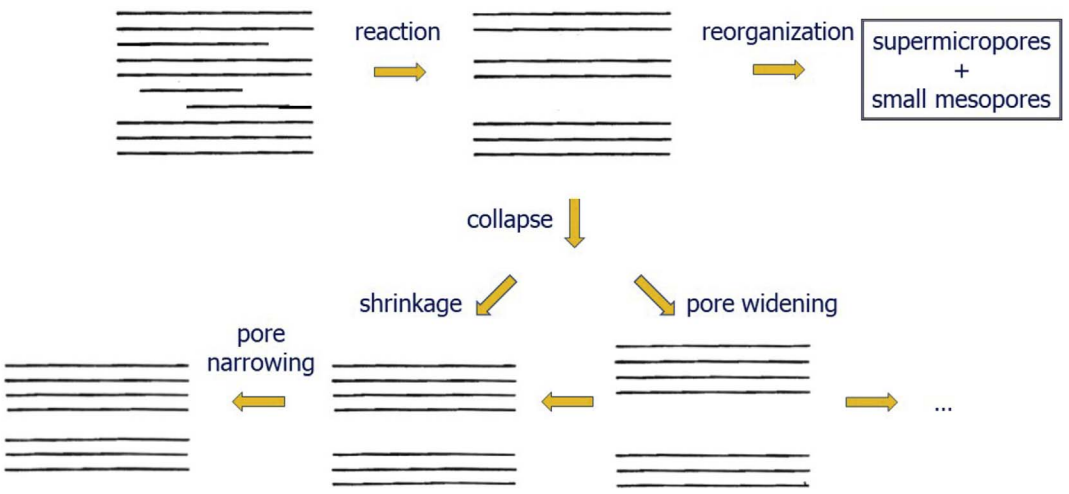

Fig. 3. Model for the evolution of pore structure during activation (adapted from Ref. [21]).

Considering similar levels of burn-off the values of the parameters related to surface area or pore volume, namely A_{BET}, A_s, v_s and v_o, are generally higher after activation at 1000 °C and lower after activation at 700 °C, although the differences are relatively small. Much more significant variations in the values of these parameters, increasing in all cases, are found as a function of burn-off. Thus, a very high value of BET area, 2064 $m^2 g^{-1}$, and total pore volume, 1.15 $cm^3 g^{-1}$, are observed for the highest burn-off sample prepared at 1000°C (FX1078) with only 90 min of activation time. The values of specific external surface area, A_s, are practically constant for samples prepared at 700 and 800 °C, while for activation at 900 and 1000°C they increase somewhat with increasing burn-off. The values of total pore volume, v_s, obtained by the α_s method, agree in all cases within ± 0.02 $cm^3 g^{-1}$ with the volume of pores up to 4 nm in width estimated by the QSDFT method, that is, with the sum of the corresponding values in columns 5 and 6 of Table 1. Finally, the values of v_o, estimated by the DA method, are much higher than the corresponding values of ultramicropore volume estimated by the QSDFT method. This confirms the findings of a previous comparison of the DA and QSDFT analyses that the DA estimate of micropore volume, v_o, includes pores of width greater than 0.7 nm [22].

Two of the parameters in Table 2, namely L_o and C, are more closely related to mean pore size and these do show significant variations as a function of activation temperature. For each activation temperature L_o increases with burn-off and, at fixed burn-off L_o increases with activation temperature. The C parameter decreases with increasing burn-off and with increasing activation temperature. At high levels of burn-off C always has comparatively low values whereas at lower levels of burn-off large variations between different activation temperatures are found, leading to high C values. For instance, when the burn-off is 29%, C varies from 537 for activation at 1000 °C up to 2289 for activation at 800°C. In summary, the variations in the values of both L_o and C indicate that mean pore size increases with increasing burn-off and that activation at low temperature results in materials with narrower pores while activation at high temperature results in materials with a broader distribution of pore sizes. The values of the DA exponent, n, are also in agreement with this. Values only slightly higher than 2 are obtained at high burn-off for all activation temperatures, whereas at low burn-off the n values vary from about 2.5 for activation at 1000 °C up to 3–4 for activation at 800 and 700°C. It has been shown that higher values of n correspond to narrower pore size distributions [23]. Hence, the n values obtained here are consistent with the other parameters discussed above in indicating a more homogeneous distribution of micropores at the lower temperatures.

For levels of burn-off below about 50%, the results obtained in this work are similar to those obtained previously with non-pre-oxidized fibres [6]. For example, considering the fibre F1N activated at 900 °C from the previous work, at fixed burn-off the values of v_s and A_{BET} are the same while the values of L_o and v_o obtained in this work are only slightly lower, by about 0.1 nm and 0.05 $cm^3 g^{-1}$, respectively. On the other hand, different behaviour is found for burn-offs greater than 50%. With the non-pre-oxidized fibre, the values of v_s, v_o and A_{BET} reached maximum values of 0.60 $cm^3 g^{-1}$, 0.47 $cm^3 g^{-1}$ and 1284 $m^2 g^{-1}$, respectively, and then decreased at higher burn-off. In the present work there was a monotonic increase up to the highest burn-off in all cases. For activation at 900 °C, this resulted in values of v_s, v_o and A_{BET} increasing up to 0.87 $cm^3 g^{-1}$, 0.61 $cm^3 g^{-1}$ and 1942 $m^2 g^{-1}$, respectively, that is, considerably higher than found previously. This considerable increase in porosity has allowed materials which are now highly comparable with current commercial products to be obtained. The great majority of commercial ACF are prepared from PAN, cellulosic, phenolic and pitch precursors and have apparent specific surface areas determined by the BET method of between 1000 and 2000 $m^2 g^{-1}$, in most cases [5]. The majority of the values of A_{BET} in Table 2 fall within this range and in one case the value is even superior to 2000 $m^2 g^{-1}$. Furthermore, these samples span a wide range of mean micropore size from about 0.8 to 1.8 nm and with short activation times of only 60 min or less in some cases.

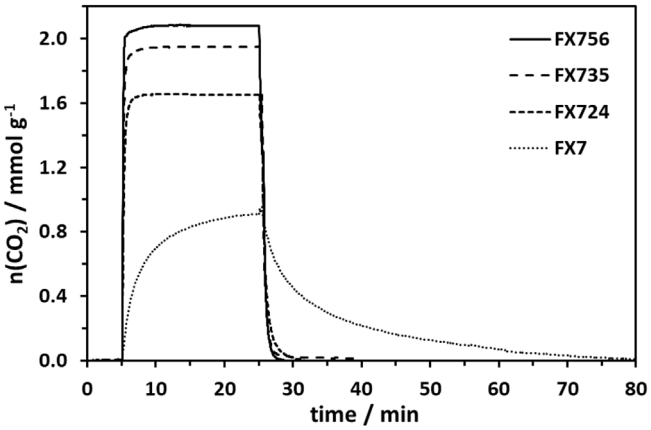

Fig. 4. Adsorption-desorption of CO_2 at 51 kPa partial pressure and 25°C.

3.3. CO_2 capture

More information about ultramicroporosity can be obtained from the adsorption of CO_2 at a temperature higher than the 77 K used for the determination of N_2 isotherms [24]. In the present work, the thermogravimetric method was used to measure the adsorption of CO_2 at 25°C and a low CO_2 partial pressure of 51 kPa. The adsorption-desorption behaviour is shown in Fig. 4 for samples carbonized and activated at 700°C and is qualitatively similar to that obtained with the materials obtained at other temperatures. It can be seen that adsorption by the activated materials is very rapid, reaching adsorption equilibrium after only a few minutes. Desorption is equally rapid with the mass returning to the initial mass also after only a few minutes. With the carbonized sample, on the other hand, adsorption equilibrium was not reached after 20 min and complete desorption was only complete after 60 min.

The amounts of CO_2 adsorbed by the materials at 25 °C and 51 kPa, obtained in each case from the plateau of the corresponding adsorption-desorption curve, are shown in Fig. 5 as a function of burn-off and it can be seen that there is a systematic variation in the values obtained. For all activation temperatures the CO_2 adsorption reaches a maximum at about 50% burn-off. The variation is most pronounced for the materials activated at 700°C and least for those activated at 1000°C. As a result, the highest amounts of CO_2 adsorbed are obtained with the samples FX756 and FX735 and the lowest (excepting the only carbonized samples) with the samples activated at 1000°C. Other work has indicated

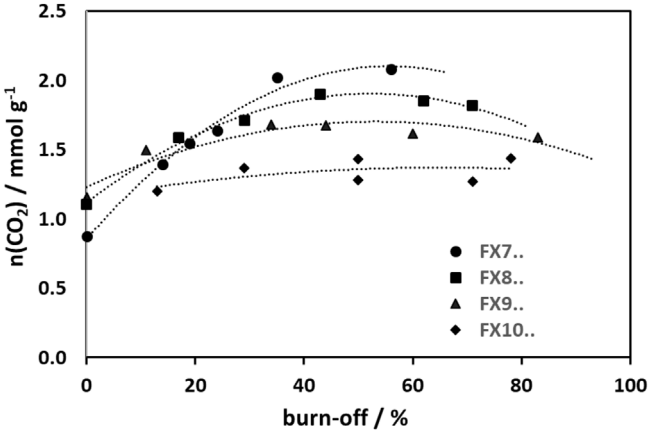

Fig. 5. CO_2 adsorbed amounts at 51 kPa partial pressure and 25°C obtained in each case from the plateau of the corresponding adsorption-desorption curve. Dotted lines are quadratic tendency lines.

that a high volume of small micropores is necessary for maximising CO_2 adsorption at low pressure [10–12], but that a high surface area can be beneficial at high pressure [25,26]. Our results suggest that, at the low pressure we used, the former is dominant. For instance, the lowest CO_2 adsorption values are given by the samples prepared at 1000°C for which the volumes of ultramicropores (Table 1) found by adsorption of N_2 at 77 K are lower and this could explain, at least partially, the lower CO_2 adsorption in comparison with the samples activated at lower temperatures. On the other hand, the 900, 800 and 700°C activated samples had very similar ultramicropore volumes by N_2 adsorption at 77 K. For these samples the differences in CO_2 adsorption may be due to differences in the distribution of ultramicropore sizes. On this basis, the results indicate that the 700°C activated samples had the highest proportion of very narrow ultramicropores and that the distribution of ultramicropore sizes shifted or broadened to higher sizes (but still $<$ 0.7 nm) as the activation temperature increased.

For a CO_2 pressure of about 100 kPa and at 25°C, a number of authors [11–16] have reported CO_2 capacities of 4–5 mmol g^{-1} and there is also one report of a CO_2 capacity of 5.5 mmol g^{-1} at 50°C from a CO_2/N_2 (15:85 v/v) mixture [27]. These results have mostly been obtained with materials prepared from synthetic polymers or mesophase pitch and using chemical activation with KOH. The highest value we have found for adsorption of CO_2 at 25°C by KOH activated acrylic fibres is 4.4 mmol g^{-1} at a CO_2 pressure of about 100 kPa [14]. Fig. 4 of reference [14] indicates that at a CO_2 pressure of about 51 kPa, the CO_2 adsorption was about 2.5 mmol g^{-1}, that is, only slightly higher than the best result, 2.1 mmol g^{-1}, obtained in this work with the sample FX756 using a CO_2 partial pressure of 51 kPa in a CO_2/N_2 mixture.

4. Conclusions

The results obtained show that pre-oxidation of acrylic fibres was effective in increasing the carbon yield during carbonization and reducing the reactivity of the char with CO_2 during activation. In addition, it was possible to obtain activated carbon fibres with significantly higher pore volumes than previously obtained with non-pre-oxidized fibres, even without a prior stabilization step, thereby contributing towards reduced production costs for the ACF manufacturer. By controlling the activation temperature and time it was possible to obtain a range of materials varying from those which contained mainly ultramicropores, with a high capacity for the capture of CO_2, up to others with a broader distribution of pore sizes extending up to 4 nm. An interesting aspect of the results was the observation that the volume of ultramicropores was practically constant for different activation times and temperatures up to 900°C.

Acknowledgements

FISIPE SA (Portugal, Member of SGL Group - The Carbon Company) is thanked for the preparation of the precursor fibre. The work was partially financed by the Fundação para a Ciência e Tecnologia (FCT, Portugal) with National (OE) funds (project UID/QUI/0619/2016).

References

[1] J. Chen, Activated Carbon Fiber and Textiles, Woodhead Publishing, Duxford, 2016.
[2] A. Linares-Solano, D. Cazorla-Amorós, Activated carbon fibers, in: S. Somiya (Ed.), Handbook of Advanced Ceramics, Academic Press, Amsterdam, 2013, pp. 155–169.
[3] J.Y. Chen, Introduction, in: J. Chen (Ed.), Activated Carbon Fiber and Textiles, Woodhead Publishing, Duxford, 2016, pp. 3–20.
[4] S.-J. Park, G.-Y. Heo, Precursors and manufacturing of carbon fibers, in: S.-J. Park (Ed.), Carbon Fibers, Springer, 2015, pp. 31–66.
[5] Z. Yue, J. Economy, Carbonization and activation for production of activated carbon fibers, in: J. Chen (Ed.), Activated Carbon Fiber and Textiles, Woodhead Publishing, Duxford, 2016, pp. 61–139.
[6] P.J.M. Carrott, J.M.V. Nabais, M.M.L. Ribeiro Carrott, J.A. Pajares, Preparation of activated carbon fibres from acrylic textile fibres, Carbon 39 (2001) 1543–1555.
[7] S. Choi, J.H. Drese, C.W. Jones, Adsorbent materials for carbon dioxide capture from large anthropogenic point sources, ChemSusChem 2 (2009) 796–854.
[8] D.M. D'Alessandro, B. Smit, J.R. Long, Carbon dioxide capture: prospects for new materials, Angew. Chem. 49 (2010) 6058–6082.
[9] N. Hedin, L. Chen, A. Laaksonen, Sorbents for CO_2 capture from flue gas—aspects from materials and theoretical chemistry, Nanoscale 2 (2010) 1819–1841.
[10] N.P. Wickramaratne, M. Jaroniec, Importance of small micropores in CO_2 capture by phenolic resin-based activated carbon spheres, J. Mater. Chem. 1 (2013) 112–116.
[11] M.E. Casco, M. Martínez-Escandell, J. Silvestre-Albero, F. Rodríguez-Reinoso, Effect of the porous structure in carbon materials for CO_2 capture at atmospheric and high-pressure, Carbon 67 (2014) 230–235.
[12] Z. Zhang, J. Zhou, W. Xing, Q. Xue, Z. Yan, S. Zhuo, S.Z. Qiao, Critical role of small micropores in high CO_2 uptake, Phys. Chem. Chem. Phys. 15 (2013) 2523–2529.
[13] J. Choma, K. Stachurska, M. Marszewski, M. Jaroniec, Equilibrium isotherms and isosteric heat for CO_2 adsorption on nanoporous carbons from polymers, Adsorption 22 (2016) 581–588.
[14] W. Shen, S. Zhang, Y. He, J. Lib, W. Fan, Hierarchical porous polyacrylonitrile-based activated carbon fibers for CO_2 capture, J. Mater. Chem. 21 (2011) 14036–14040.
[15] Y. Boyjoo, Y. Cheng, H. Zhong, H. Tian, J. Panc, V.K. Pareek, S.P. Jiang, J.F. Lamonier, M. Jaroniec, J. Liu, From waste Coca Cola® to activated carbons with impressive capabilities for CO_2 adsorption and supercapacitors, Carbon 116 (2017) 490–499.
[16] N.P. Wickramaratne, M. Jaroniec, Activated carbon spheres for CO_2 adsorption, ACS Appl. Mater. Interfaces 5 (2013) 1849–1855.
[17] A.V. Neimark, L. Yangzheng, P.I. Ravikovitch, M. Thommes, Quenched solid density functional theory and pore size analysis of micro-mesoporous carbons, Carbon 47 (2009) 1617–1628.
[18] F. Rouquerol, J. Rouquerol, K.S.W. Sing, Adsorption by Powders and Porous Solids, Academic Press, London, 1999.
[19] M. Thommes, K. Kaneko, A.V. Neimark, J.P. Olivier, F. Rodríguez-Reinoso, J. Rouquerol, K.S.W. Sing, Physisorption of gases, with special reference to the evaluation of surface area and pore size distribution (IUPAC Technical Report), Pure Appl. Chem. 87 (2015) 1051–1069.
[20] H.F. Stoeckli, P. Rebstein, L. Ballerini, On the assessment of microporosity in active carbons, a comparison of theoretical and experimental data, Carbon 28 (1990) 907–909.
[21] P.J.M. Carrott, J.J. Freeman, Evolution of micropore structure of activated charcoal cloth, Carbon 29 (1991) 499–506.
[22] P.J.M. Carrott, M.M.L. Ribeiro Carrott, Suhas, Comparison of the Dubinin-Radushkevich and Quenched Solid Density Functional Theory approaches for the characterisation of narrow microporosity in activated carbons obtained by chemical activation with KOH or NaOH of Kraft and hydrolytic lignins, Carbon 48 (2010) 4162–4169.
[23] P.J.M. Carrott, M.M.L. Ribeiro Carrott, Evaluation of the Stoeckli method for the estimation of micropore size distributions of activated charcoal cloths, Carbon 37 (1999) 647–656.
[24] J. Jagiello, M. Thommes, Comparison of DFT characterization methods based on N_2, Ar, CO_2, and H_2 adsorption applied to carbons with various pore size distributions, Carbon 42 (2004) 1227–1232.
[25] Z. Yong, V. Mata, A.E. Rodrigues, Adsorption of carbon dioxide at high temperature - a review, Separ. Purif. Technol. 26 (2002) 195–205.
[26] S. Himeno, T. Komatsu, S. Fujita, High-pressure adsorption equilibria of methane and carbon dioxide on several activated carbons, J. Chem. Eng. Data 50 (2005) 369–376.
[27] H.Y. Hsiao, C.M. Huang, M.Y. Hsu, H. Chen, Preparation of high-surface-area PAN-based activated carbon by solution-blowing process for CO_2 adsorption, Separ. Purif. Technol. 82 (2011) 19–27.